RZ 3483 (# 93757) 02/17/03
Electrical Engineering 7 pages

Research Report

Performance of Binary Antipodal Signaling over the Indoor UWB MIMO Channel

Martin Weisenhorn and Walter Hirt

IBM Research
Zurich Research Laboratory
8803 Rüschlikon
Switzerland
{mwe,hir}@zurich.ibm.com

Performance of Binary Antipodal Signaling over the Indoor UWB MIMO Channel

Martin Weisenhorn
IBM Research, Zurich Research Laboratory
CH-8803 Rüschlikon, Switzerland
Email: mwe@zurich.ibm.com

Walter Hirt
IBM Research, Zurich Research Laboratory
CH-8803 Rüschlikon, Switzerland
Email: hir@zurich.ibm.com

***Abstract*— We generalize a suitable, known indoor UWB SISO channel model to obtain a new discrete-time model for the indoor UWB MIMO radio channel. The properties and potential benefits arising from the channel's specific correlation features are investigated by means of simulations. We show that the indoor UWB channel can offer much lower ISI than would be expected for a given rms delay spread, and confirm that systems operating on this channel require a small-scale fading margin of only a few dB. It is further demonstrated that an uncoded MIMO communication scheme applied to the UWB channel can offer superior SVEP performance compared to its use on the i.i.d. Rayleigh flat fading channel. Moreover, it was found that such an UWB scheme can offer very low SVEP with several transmitting and only a single receiving antenna (MISO), in contrast to a similar narrowband system.**

I. Introduction

The recent initiative taken by the US-based Federal Communications Commission (FCC) to regulate the use of commercial ultra-wideband (UWB) radio devices has spurred a growing interest for this emerging technology in industrial as well as academic research institutions [1]–[3]. As the FCC's UWB spectrum masks and related specifications were published only recently, characterization and modelling of the UWB radio channel as well as the assessment of fundamental system design and performance issues continue to be of importance, particularly for the indoor environment. In practice, the FCC spectrum mask confines emissions from UWB radio devices to the frequency range of 3.1 to 10.6 GHz, offering 7.5 GHz of continuous spectrum. In this range, the average of the EIRP (effective isotropically radiated power) is limited to the value obtained from the product of the signal's -10 dB bandwidth, $B > 500$ MHz, and the maximal power spectral density, -41.3 dBm/MHz, corresponding to 75 nW/MHz [1]. Thus by their very definition, UWB radio systems are severely limited in terms of transmitted power but excessive in their use of bandwidth.

In the past, assuming different channel models and modulation schemes, various UWB communication systems and their performance were investigated and reported. The principle of UWB impulse radio and some aspects of the UWB indoor channel are described in [4] and [5], respectively. Time-hopping pulse position modulation (PPM) over a measured channel is considered in [6], binary PPM in connection with a Nakagami fading channel model is investigated in [7], and the corresponding channel model is presented in [8]. Reference [9] deals with time-hopping PPM and a two-path Rayleigh fading channel, and [10] assesses space-time coding for impulse radio systems assuming a Rayleigh flat fading (RFF), multiple-input/multiple-output (MIMO) channel. A form of UWB multiple access communication is described in [11]. Finally, unlike narrowband radio systems, properly designed UWB radio systems have been shown to suffer less from fading effects, because the extremely narrow pulses propagating on different paths cause a large number of independently fading signal components that can be resolved in time, therefore the channel offers high multipath diversity [6].

In this paper, we focus on the specific properties of the indoor UWB MIMO channel itself and assess their impact on the potential performance of various MIMO communication systems using binary antipodal modulation. Section II introduces a simple, uncoded MIMO communication system consisting of M independent binary modulators (one for each transmitting antenna), an UWB MIMO channel or the RFF MIMO channel, and a receiver using a sampled matched filter followed by a maximum-likelihood (ML) symbol-vector detector that accounts for interchannel interference (ICI) but ignores intersymbol interference (ISI). In Section III we adopt the single-input/single-output (SISO) UWB indoor channel model proposed in [12] and generalize it to the indoor UWB MIMO channel model as used in this paper. In Section IV we describe the correlation properties of channels generated according to the proposed indoor UWB channel model and study their impact on the performance of UWB MIMO communication systems. Finally, in Section V we compare the symbol-vector error probability (SVEP) of MIMO communication systems for the UWB channel, the RFF channel, and the respective specializations to the SISO communication system. We also explain the reason for the reduced small-scale fading margin of the UWB channel reported in [6] and [13], and confirm this with simulation results. Furthermore, we point out the potential for obtaining much lower ISI on the indoor UWB channel than would be expected for a given rms delay spread, and demonstrate it with simulation results. It turns out that, in contrast to the RFF channel, the UWB channel allows a remarkable SVEP performance even when the number of transmitting antennas exceeds the number of receiving antennas.

II. System Model

The MIMO communication system depicted in Fig. 1 employs M transmitting and N receiving antennas. Uncoded communication is used; therefore, there are M parallel data streams at the transmitter side, indexed by the numbers $1, 2, \ldots, m, \ldots, M$. Antipodal binary symbols $a_{mk} \in \{-1, +1\}$ are transmitted in the m-th data stream at time index k, which can be collected into vectors $\mathbf{a}_k \triangleq (a_{1k}, \ldots, a_{Mk})^T$. Using this definition, the input signal $\mathbf{u}(\mathbf{t})$ to the system given in Fig. 1 is described by

$$\mathbf{u}(t) = \sum_{k=0}^{K-1} \mathbf{a}_k \ \delta(t - kT_s), \tag{1}$$

where K denotes the number of symbol vectors associated with a transmitted data block and T_s is the symbol duration; accordingly, the pulse repetition frequency (PRF) is defined as $R_s \triangleq 1/T_s$. A quasi static channel is assumed, which implies the channel to be time invariant during the transmission of one data block. All continuous time signals, with the exception of $\mathbf{u}(t)$, will be given in equivalent baseband representation. This, in combination with the definition of the passband transform, $s'(t) = \Re\left\{s(t)e^{j2\pi f_0 t}\right\}$, is the reason for the factor $\frac{1}{2}$ in the subsequent calculations of correlation functions and convolutions. The signal $\mathbf{u}(t)$ is filtered by the pulse-shaping

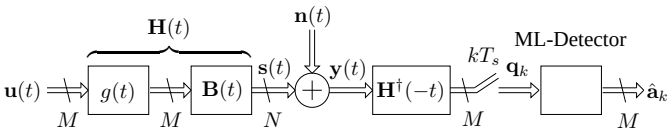

Fig. 1. UWB MIMO communication system model.

filter $g(t)$, whose Fourier transform is a cosine roll-off function with parameter $\alpha = 0.1$ [14]. To assess the impact of both the minimum and maximum signal bandwidths allowed, we consider two different filter bandwidths, $B = 500$ MHz and $B = 7.5$ GHz, each measured at the -10 dB roll-off points in compliance with [1]. The resulting matrix of received pulse shapes is defined as

$$\mathbf{H}(t) \triangleq \frac{1}{2}\mathbf{B}(t) * g(t), \tag{2}$$

representing the convolution of the channel impulse response matrix, $\mathbf{B}(\mathbf{t})$, with the pulse-shaping filter, $g(t)$. Owing to its large signal bandwidth B, $g(t)$ is a short pulse with a duration on the order of 1 ns. The noisy received signal $\mathbf{y}(t) = \mathbf{s}(t) + \mathbf{n}(t)$ has dimension N, and $\mathbf{n}(t)$ is a white Gaussian noise vector with two-sided power spectral density N_0 and autocorrelation function (ACF) $\frac{1}{2}\mathbb{E}\left\{\mathbf{n}(t+\tau)\mathbf{n}(t)^\dagger\right\} = N_0\mathbf{I}_N\delta(\tau)$, $\mathbf{I}_N$ being the unity matrix.

The aim of this paper is to show the potential performance for the transmission of antipodal binary modulated signals over the UWB MIMO channel. As the performance measure we use the mean SVEP, $\overline{\text{SVEP}} \triangleq \mathbb{E}\{\text{SVEP}\}$, which is minimized by the use of a ML symbol-vector detector [15]. To keep the ML detector simple, the channel is assumed to cause interference only between the components of the signal vector $\mathbf{s}(t)$ in the form of interchannel interference (ICI). Thus, interference between adjacent symbol vectors is not considered, and no intersymbol interference (ISI) is assumed.

A very simple ML detector can be realized, when providing it with the sampled matched filter outputs, $\mathbf{q}_k$, which represent a sufficient statistics for ML detection [15]. Thus, because of (2), implementation of the matched filter matrix $\mathbf{H}^\dagger(-t)$, which is the conjugate transpose of $\mathbf{H}(-t)$, requires perfect knowledge of the channel impulse response matrix $\mathbf{B}(t)$. Based on Fig. 1 and Eq. (1), the sample vectors $\mathbf{q}_k$ can be written as

$$\mathbf{q}_k = \sum_i \mathbf{W}_{k-i} \ \mathbf{a}_i \ + \ \mathbf{z}_k, \tag{3}$$

where

$$\mathbf{W}_j \triangleq \frac{1}{2}\int \mathbf{H}^\dagger(t - jT_s) \ \mathbf{H}(t) \ dt, \tag{4}$$

and $\mathbf{z}_k$ is a noise vector with Gaussian-distributed components and autocorrelation matrix $\frac{1}{2}\mathbb{E}\{\mathbf{z}_{j+l}\mathbf{z}_l^\dagger\} = N_0\mathbf{W}_j$. This representation is known as the equivalent discrete channel description [16]; it will later also be used to explain various interference effects. The matched filter used in the simulations is a discrete-time filter with a tap spacing corresponding to the Nyquist sampling rate. For the assumed -10 dB signal bandwidths $B = 500$ MHz and 7.5 GHz, the matched filter corresponds to a Rake receiver frontend with 86 and 1288 taps, respectively [17].

III. The Channel Model

We chose the channel model presented in [12] because it appears to be the only available UWB (SISO) channel model that allows the spatial position of the transmitting and receiving antennas to be specified, which is a prerequisite for the generation of MIMO channel realizations. A peculiarity of this channel model is that it assumes a certain number, V, of virtual sources distributed in space. Each virtual source corresponds to a reflecting object and causes a propagation path with an associated specific path impulse response that is independent of the receiver and transmitter position. Delay and attenuation of the received signal depend on the distance between the corresponding virtual source and the receiver. Consequently, a channel impulse response is the superposition of V weighted and time-shifted path impulse responses. The individual path impulse responses in turn are represented as discrete-time signals consisting of Rayleigh-distributed tap coefficients, whose energy decays exponentially with time. These signals then are passed through a filter to account for the $1/f$ amplitude gain of very wideband channels. The phase of the tap coefficients is uniformly distributed in $[-\pi, \pi)$; for more details on this channel model, see [12] and [18].

In the channel model, the positions of the virtual sources depend on the room dimensions, on the transmitter but not the receiver position, and on parameters that describe the reflecting objects and are extracted from underlying channel measurement data. In reality, however, the position of a virtual source not only depends on the transmitter position, but also on the receiver position. As described below, the variations in the

receiver and transmitter positions will be relatively small, such that the impact of the receiver position on the position of the virtual sources will also be small. In practice, the intensity of a reflected signal will also vary with the angle of the incoming wave; this effect is also ignored in the channel model. However these simplifications have little impact on the channel impulse responses generated.

As is commonly assumed for narrowband indoor channels, we also assume the UWB channel to be quasi-static [19]. We describe the MIMO channel by the channel impulse response matrix $\mathbf{B}(t)$, whose components are SISO channel impulse responses $[\mathbf{B}(t)]_{nm} = b_{nm}(t)$, where n and m are the receiving antenna and transmitting antenna indices, respectively. We generalize the SISO channel model [12] to the MIMO scenario by assuming the same path impulse responses associated with the virtual sources for every channel impulse response $b_{nm}(t)$. From a more realistic viewpoint, this simplifying assumption will likely lead to a somewhat conservative model; subsequently, we will discuss the effect of this assumption on the simulation results.

From the various usage scenarios listed in [12], we decided to adopt the communication link from one office to an adjacent one. This link scenario uses $V = 12$ virtual sources, yielding a dense multipath channel with an rms (root mean square) delay spread, $\tau_{\text{rms}}(n,m)$, of approximately 13 ns for all combinations of n and m, where

$$\tau_{\text{rms}}(n,m) \triangleq \sqrt{\frac{\int (t-\bar{t})^2 |b_{nm}(t)|^2 dt}{\int |b_{nm}(t)|^2 dt}}, \quad \bar{t} \triangleq \frac{\int t\ |b_{nm}(t)|^2 dt}{\int |b_{nm}(t)|^2 dt}.$$

The linear arrays of M transmitting and N receiving antennas are arranged on a 10 cm and 5 cm grid, respectively, where it is assumed that the individual array elements are entirely decoupled. In Fig. 2, a MIMO communication system with $M = 3$ transmitting and $N = 2$ receiving antennas is shown.

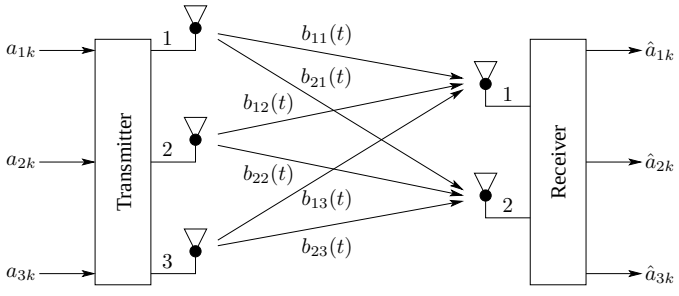

Fig. 2. MIMO communication system with $M = 3$ transmitting and $N = 2$ receiving antennas.

Realizations of the corresponding passband channel impulse responses $b'_{nm}(t)$ in response to an ideal passband pulse with center frequency $f_c = 6.85$ GHz and bandwidth $B = 7.5$ GHz are depicted in Fig. 3.

If we decrease the signal bandwidth B to a few tens of MHz, then, under some well-known restricting assumptions, the UWB channel degenerates to the i.i.d. MIMO RFF channel and the equivalent discrete channel $\mathbf{W}_j = \tilde{\mathbf{H}}^{\dagger}\tilde{\mathbf{H}}\,\delta_j$ for a channel realization $\tilde{\mathbf{H}}$, where δ_j is the Kronecker symbol [16].

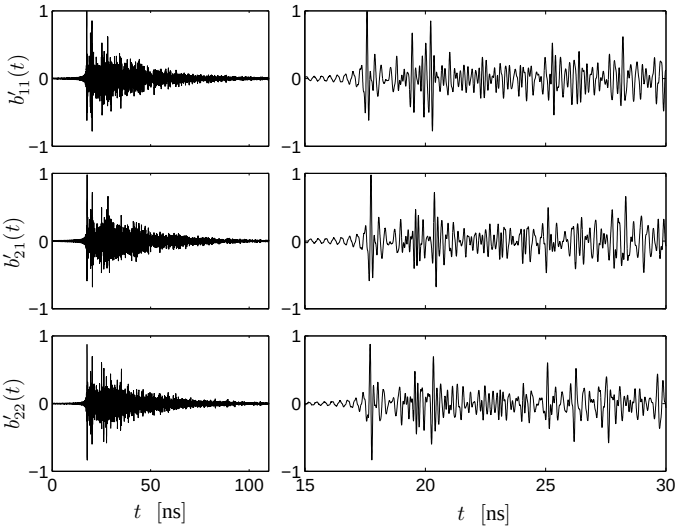

Fig. 3. Typical realizations of indoor UWB MIMO channel impulse responses in passband representation, generated according to the MIMO channel model ($f_c = 6.85$ GHz, $B = 7.5$ GHz).

IV. Crosscorrelation Function of the Received Pulse Shapes

We can write (4) componentwise as

$$[\mathbf{W}_j]_{lr} = \frac{1}{2}\sum_{n=1}^{N} \phi_{h_{nl}h_{nr}}(jT_s),$$

with the correlation functions $\phi_{h_{nl}h_{nr}}(\tau) \triangleq \int h^{\dagger}_{nl}(t)h_{nr}(t+\tau)dt$ and with $h_{nm}(t) = [\mathbf{H}(t)]_{nm}$. With this and (3) we observe that crosscorrelations, i.e., $\phi_{h_{nl}h_{nr}}(0) \neq 0$, for $l \neq r$, cause ICI through interference between components of the symbol vector $\mathbf{a}_k$, whereas crosscorrelations $\phi_{h_{nl}h_{nr}}(\tau) \neq 0$, for $|\tau| \geq T_s$ cause ISI through interference between components of symbol vectors $\mathbf{a}_k$ with different time indices k. To obtain deeper insight into the correlation properties of the UWB channel, we consider the baseband pulse shapes $h_{11}(t)$ and $h_{12}(t)$ received from antenna $n = 1$, when a pulse $g(t)$ is transmitted from the fixed reference antenna, $m = 1$, and a moving second antenna, $m = 2$, respectively. Let the deviation in the position of the second transmitting antenna relative to the reference antenna be $\Delta_d > 0$, implying a displacement of the second transmitting antenna towards the receiving antenna. The resulting absolute value of the deterministic and normalized baseband crosscorrelation function (CCF),

$$\varphi_{h_{11}h_{12}}(\tau, \Delta_d) \triangleq \frac{|\phi_{h_{11}h_{12}}(\tau)|}{\sqrt{\int |h_{11}(t)|^2 dt}\ \sqrt{\int |h_{12}(t)|^2 dt}}, \qquad (5)$$

for a specific channel realization is depicted in Figs. 4 and 5 for pulse-shaping filter bandwidths $B = 7.5$ GHz and 500 MHz, respectively. Especially in Fig. 4, some prominent properties can be observed. For $\Delta_d = 0$, the CCF in (5) degenerates to the autocorrelation function (ACF) $\varphi_{h_{11}}(\tau)$ of the received pulse shape $h_{11}(t)$. It can be seen that $\varphi_{h_{11}}(\tau)$ is very narrow compared to the rms delay spread of about 13 ns, i.e., for

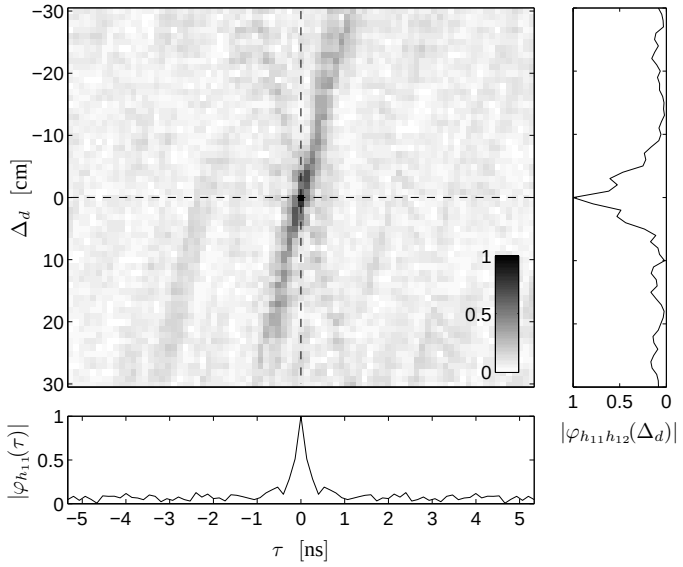

Fig. 4. Absolute values of CCF and ACF (CCF at $\Delta_d = 0$) of received pulse shape realizations $h_{11}(t)$ and $h_{12}(t)$ for $B = 7.5$ GHz.

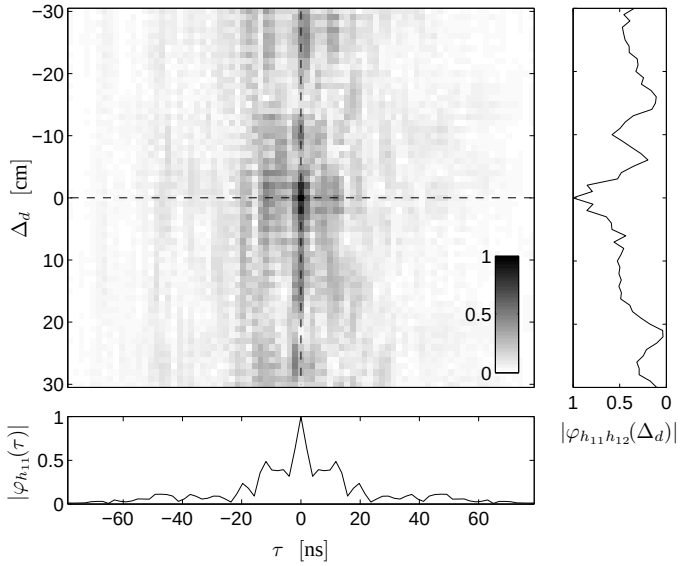

Fig. 5. Absolute values of CCF and ACF (CCF at $\Delta_d = 0$) of received pulse shape realizations $h_{11}(t)$ and $h_{12}(t)$ for $B = 500$ MHz.

$\tau = 0.5$ ns, its magnitude is already reduced to about 0.2. This property results from the large number of resolvable signal components and their random phase. This suggests an interpretation of the discrete-time received pulse shapes $h_{nm}(nT)$ as randomly coded complex sequences. For $\tau = 0$, the CCF in (5) degenerates to the function $\varphi_{h_{11}h_{12}}(\Delta_d)$, which describes the ICI behavior as discussed above.

The predominant diagonal line in Fig. 4 has a slope of -30 cm/ns due to the free-space propagation velocity of 3×10^8 m/s. Thus, introducing a Δ_d on the order of only a few centimeters causes $h_{11}(t)$ to be correlated with a significantly time-shifted version of $h_{12}(t)$. The larger the offset Δ_d, the less correlated $h_{11}(t)$ becomes with the time-shifted version of $h_{12}(t)$. The weak diagonal lines in Fig. 4 stem from the path impulse responses, induced by the virtual sources of the channel model, present in every channel impulse response $b_{nm}(t)$ [12]. The maximum number of diagonal lines in a CCF equals the number of virtual sources. Clearly, removing our conservative assumption that the path impulse responses are the same for all transmitter and receiver positions would lead to an even narrower CCF with respect to τ and would make the weak diagonal lines in Fig. 4 even weaker. The CCF of the same channel is depicted in Fig. 5, assuming a bandwidth of only 500 MHz for the transmitted pulse $g(t)$; as expected, for this reduced bandwidth, the achievable space-time resolution is much smaller.

V. Simulation Results

In this section we compare the performance of communication systems with different signal bandwidths B, where very small bandwidths justify the use of the RFF channel model, as indicated before. Hence, differences in the properties of UWB and narrowband communication systems become apparent.

In what follows we compare transmitters with different numbers of antennas, M, and corresponding symbol vectors. Because of symmetry considerations, all symbols of a detected symbol vector show the same error probability; however, their joint error statistics will show some degree of correlation. A detected symbol vector, $\hat{\mathbf{a}}_k$, is in error if at least one of its symbols is incorrect. Consequently, the SVEP will be higher than the SEP and increase with M. Thus, it would be unfair to compare the SVEP of systems with different M. We solve this conflict by stacking detected symbol vectors $\hat{\mathbf{a}}_k$ to obtain vectors $(\hat{\mathbf{a}}_k^T, \hat{\mathbf{a}}_{k+1}^T, \ldots)^T$, such that they contain the same number, L, of symbols for all communication systems to be compared in the same figure, where L is the least common multiple of all Ms used. We shall denote the respective error probabilities as SVEP_L, when considering exclusively SISO systems, we will use the term SEP instead of SVEP_1.

The communication systems under discussion are each applied to different channel realizations, leading to different SVEP values. We measure the performance of a system in terms of the estimate $\overline{\text{SVEP}} \triangleq \mathbb{E}\{\text{SVEP}\}$, where the mean value is taken over different realizations of the MIMO channel, generated by moving the receiving antenna array in a rectangular area (150 cm $\times$ 30 cm). Because of the relatively small dimensions of this area, our results reflect only the small-scale fading effects of the channel.

The total instantaneously received signal energy per receiving antenna and data symbol is given by

$$\zeta \triangleq \frac{\int \mathbf{s}^\dagger(t)\,\mathbf{s}(t)\,dt}{2\,KMN}. \tag{6}$$

Using this expression, we define the mean signal-to-noise ratio (SNR) as

$$\overline{\text{SNR}} \triangleq \frac{\overline{\zeta}}{N_0}, \tag{7}$$

where $\overline{\zeta} \triangleq \mathbb{E}\{\zeta\}$. Based on these definitions, we compare the performances of binary antipodal modulation for the AWGN

channel, the indoor UWB channel, and the RFF channel. Unless otherwise stated, the pulse $g(t)$ used to signal over the indoor UWB channel has a bandwidth of $B = 7.5$ GHz.

A. Fading Margin for the SISO Channel

Transmission over the AWGN channel leads to a constant received signal power, and thus a single channel realization suffices to determine the SEP. When transmitting over fading channels, however, the received signal energy varies with each channel realization, leading to a varying SEP around its mean value, $\overline{\text{SEP}}$. In Fig. 6, the cumulative distribution function (CDF) of the received signal energy is plotted for different channel types. We define the "fading margin" as the increase

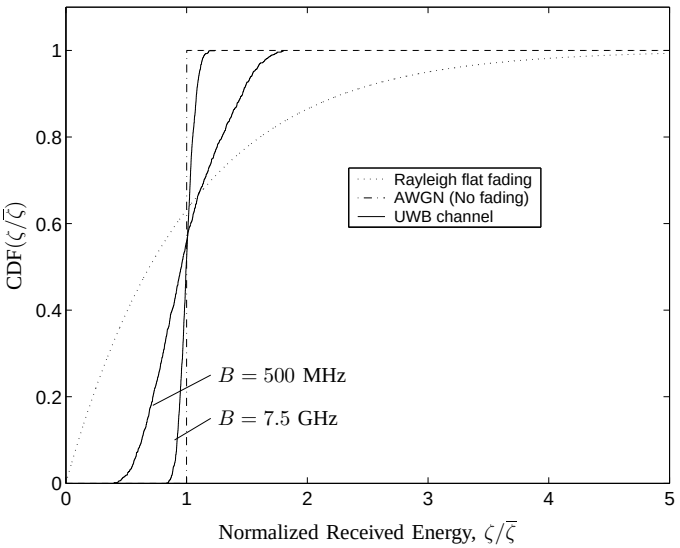

Fig. 6. Cumulative distribution functions of the received signal energy for different SISO channels.

in transmitted power, required to overcome the fading-related increase in $\overline{\text{SEP}}$. As we only model small-scale effects, we use "fading margin" to mean "small-scale fading margin". This usage is also made in [6], although other definitions exist (see, e.g., [13], [20]).

The values of $\overline{\text{SEP}}$ achieved by the systems operating over the SISO fading channels considered here exceed the SEP achieved on the AWGN channel. From Fig. 7 we see that for an $\overline{\text{SEP}} = 10^{-5}$ the fading margin for binary signaling over the indoor UWB channel with $B = 7.5$ GHz is about 0.1 dB and about 1.1 dB for $B = 500$ MHz. In contrast, transmission over the RFF channel requires a fading margin of about 35 dB. The large $\overline{\text{SEP}}$ for the RFF channel is due to the high probability of receiving only a fairly small amount of signal energy; the UWB channels, in contrast, suffer much less from this effect, see Fig 6.

B. Impact of the PRF on the $\overline{\text{SEP}}$ for the SISO Channel

The same ideal UWB SISO communication system as in Subsection V-A is used, differing only in the PRF. So far, the PRF was kept sufficiently low to avoid ISI, i.e., $R_s = \frac{1}{160\ \text{ns}}$ has been used. Under this condition, the detector in Fig. 1

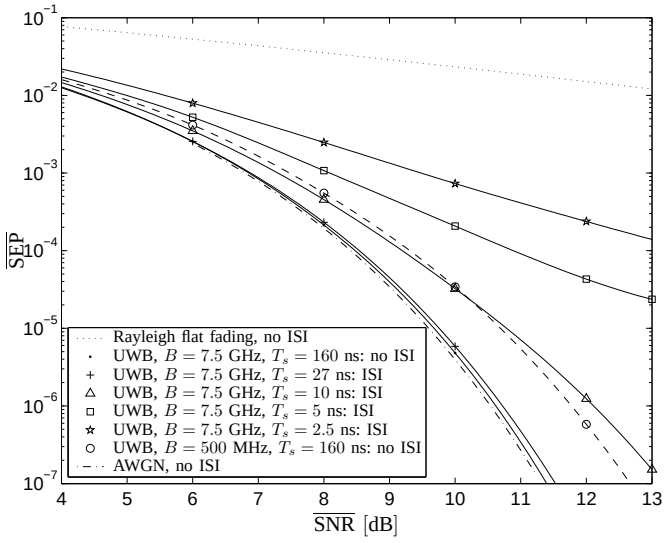

Fig. 7. Mean symbol error probabilities vs. $\overline{\text{SNR}}$ for different SISO channels.

corresponds to the ML detector as described in Section II. To study the effect of ISI, the PRF can be increased. In the presence of ISI, however, the detector no longer provides ML decisions and the receiver becomes increasingly suboptimal, with increasing ISI. From (3), it follows that the ISI effect arising from the use of a smaller symbol duration T_s is perfectly described by the matrices $\mathbf{W}_j$. For the SISO case, for example, the latter can be shown to be equivalent to the ACF, $\phi_{h_{11}}(\tau)$, sampled at time $\tau = jT_s$, i.e., $\phi_{h_{11}}(\tau)$ perfectly describes the added ISI effect. Therefore, the intensity of ISI depends on the PRF, and the faster $\phi_{h_{11}}(\tau)$ decays with increasing $|\tau|$, the fewer symbol vectors $\mathbf{a}_k$ have a significant impact on the sample vector $\mathbf{q}_k$. The peak of the ACF $\varphi_{h_{11}}(\tau)$ depicted in Fig. 4 is relatively narrow compared to the channel's rms delay spread $\tau_{\text{rms}} \approx 13$ ns. For this case, we thus expect only a small increase in $\overline{\text{SEP}}$ for PRFs up to $R_s \approx 1/\tau_{\text{rms}}$, compared to the case without ISI. This conclusion is confirmed by the simulation results depicted in Fig. 7, where at $\overline{\text{SEP}} = 10^{-5}$ for $T_s = 10$ ns, i.e., $R_s = 100$ Mb/s, the system's $\overline{\text{SEP}}$ suffers a penalty of only about 1.2 dB, compared to communication over the AWGN channel. For a PRF corresponding to $T_s = 5$ ns, i.e., $R_s = 200$ Mb/s and higher, an error floor can be observed in Fig. 7, indicating that the total amount of interference is dominated by ISI rather than noise (AWGN).

C. Transmission over the MIMO Channel

The communication system structure considered in Subsection V-A is again assumed; however, the number of transmitting and receiving antennas can now both exceed unity, i.e., a UWB MIMO system will be considered. Figure 8 compares the resulting $\overline{\text{SVEP}}$ performances of systems with various UWB MIMO channels and the i.i.d. MIMO RFF channel. When interpreting Fig. 8, note that in general, doubling the number of independently transmitting antennas, M, does not change the $\overline{\text{SNR}}$, as the received energy per symbol remains

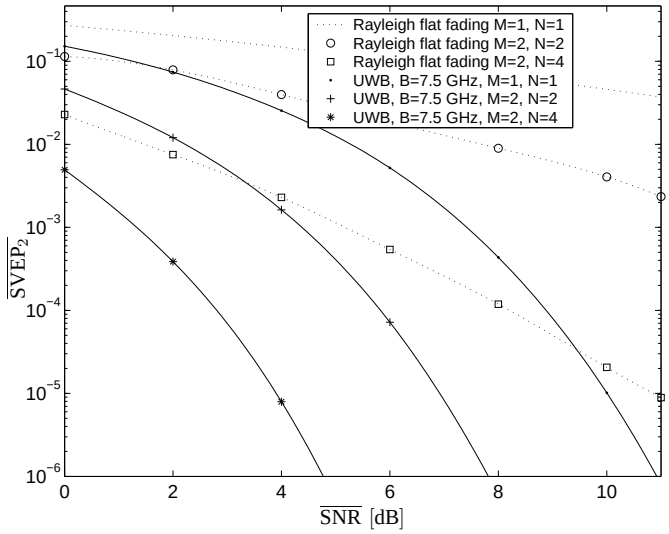

Fig. 8. Mean symbol-vector error probabilities vs. $\overline{\text{SNR}}$ for UWB and Rayleigh flat fading MIMO channels.

the same, cf. (6) and (7). On the other hand, the negative impact of the additional ICI at the individual matched filter outputs caused by increasing M is relatively small for the UWB channel. In contrast, doubling the number of receiving antennas, N, yields a 3 dB improvement in $\overline{\text{SNR}}$, because the received signal amplitudes add coherently whereas the corresponding noise components add incoherently. Moreover, this positive trend is enhanced due to the incremental diversity gain of the system.

It is well known that the diversity gain of a system operating on the RFF channel increases with the number of receiving antennas, N; this can also be seen by comparing the respective $\overline{\text{SVEP}}$ curves and their slopes in Fig. 8 [14]. As explained above, an additional detection or signal-processing gain of 3 dB is obtained when doubling the number of receiving antennas, N. On the other hand, the effect of an additional diversity gain obtained from increasing N, indicated by an increased slope of the corresponding $\overline{\text{SVEP}}$ vs. $\overline{\text{SNR}}$ curves, is not significant for the UWB system. The reason is that the diversity order of UWB systems, induced by the large number of resolvable multipaths, is already very high for each scalar received pulse shape, $h_{nm}(t)$, forming the matrix-valued MIMO channel $\mathbf{H}(t)$. Thus, for the UWB MIMO channel, the $\overline{\text{SVEP}}$ limit that can be asymptotically approached with increasing diversity order is nearly reached even for $N = 1$. The same effect can be observed in Fig. 7 for the SISO channel, where an increase in bandwidth from 500 MHz to 7.5 GHz adds only an incremental diversity gain.

The superior $\overline{\text{SVEP}}$ performance of the UWB system is obtained at the expense of a very large system bandwidth that is about two orders of magnitude greater than that for an indoor system, where flat fading can be assumed for bandwidths up to a few tens of MHz. As a consequence, the spectral efficiency $\eta = R_s M/B$, measured in units of (b/s)/Hz, of the UWB systems considered, is rather low. However, it can be improved to some degree by increasing the PRF, up to about $T_s = \tau_{\text{rms}}$, as only a marginal deterioration of $\overline{\text{SVEP}}$ results from the corresponding increase in ISI, see Fig. 7. Further improvements in terms of η could be achieved by applying QAM modulation as indicated in [16]. In passband representation this scheme corresponds to using the pulse-shaping filter $g'(t)$ as well as its Hilbert transform $\mathcal{H}\{g'(t)\}$. However, these techniques are not sufficient to achieve the rather high spectral efficiencies of known narrowband communication systems.

ISI-free communication requires $\mathbf{W}_j = \mathbf{0}$ for all $j \neq 0$. Because we use antipodal signaling, the real part of $\mathbf{W}_0$, $\Re\{\mathbf{W}_0\}$, determines the $\overline{\text{SVEP}}$ performance of the system. The CCF depicted in Fig. 4 indicates that the impulse responses $h_{1m}(t)$, received at antenna $n = 1$ when a pulse $g(t)$ is transmitted by the m-th transmitting antenna, are only weakly correlated. Thus, the autocorrelation terms, i.e., the diagonal components of $\Re\{\mathbf{W}_0\}$ should predominate, as confirmed by the numerical mean values

$$\mathbb{E}\{|\Re\{\mathbf{W}_0\}|\} \sim \begin{bmatrix} 0.99 & 0.26 \\ 0.26 & 1.01 \end{bmatrix}$$

for $M = 2$ and $N = 1$, for example. For the MIMO communication system in Fig. 1, this means that only a small amount of ICI is introduced by such a channel. It should thus be possible to successfully receive sequences of independent symbols a_{mk} over the UWB MISO channel formed by $M > 1$ transmitting antennas but only a single receiving antenna ($N = 1$). This has been confirmed by computing the $\overline{\text{SVEP}}$ as depicted in Fig. 9. As explained, increasing the number of transmitting antennas, M, introduces additional ICI. The impact of this on $\overline{\text{SVEP}}$ is relatively small for the UWB channel with $B = 7.5$ GHz, as seen in Fig. 9. Decreasing the signal bandwidth widens the CCF $\phi_{h_{nr}h_{nl}}(\tau)$; the resulting increase in ICI impacts the $\overline{\text{SVEP}}$ as indicted in Fig. 9 for $B = 500$ MHz and the narrowband RFF channel.

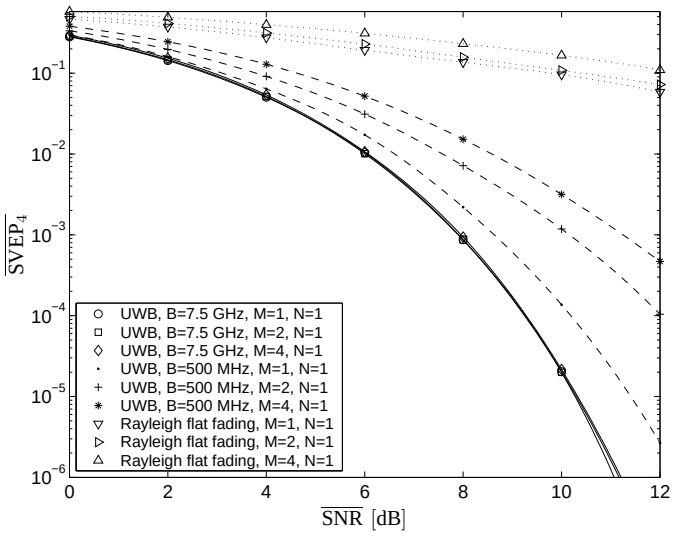

Fig. 9. Mean symbol-vector error probabilities vs. $\overline{\text{SNR}}$ for UWB and i.i.d. Rayleigh flat fading MIMO channels with M transmitting antennas and one receiving antenna ($N = 1$).

The advantage of the UWB indoor channel over the RFF channel can also be seen from the dimensions of the spaces spanned by their received pulse shape $\mathbf{H}(t)$ and $\tilde{\mathbf{H}}$, respectively. While $\tilde{\mathbf{H}}$ spans a vector space with dimension $d \leq \min\{M, N\}$, $\mathbf{H}(t)$ spans a vector-signal space with dimension $d \leq M$.

VI. Conclusion

A suitable indoor UWB SISO channel model, based on extensive as well as realistic measurements and recently reported in [12], has been generalized to obtain a new discrete-time model for the indoor UWB MIMO radio channel. The properties and potential performance of different communication systems arising from the channel's specific correlation features were investigated by means of simulations for antipodal binary modulated signals.

In particular, the results confirm that UWB systems can operate with a much reduced small-scale fading margin compared to systems operating on the (narrowband) RFF channel. It was also shown that UWB communication systems suffer much less from ISI than one would expect from inspecting the rms delay spread of the corresponding channel. Responsible for this are the favorable properties of the autocorrelation function of the received pulse shapes. On the other hand, with the diversity order of UWB channels being inherently already very large, the performance improvements by increasing the diversity through the addition of receiving antennas have been shown to be only marginal.

When compared to the corresponding SISO case, uncoded MIMO communication applied to the UWB channel was found to yield a smaller performance improvement potential than MIMO schemes applied to the RFF channel. However, we have shown that the UWB MIMO channel offers superior absolute SVEP performance, which is remarkable even if there is only a single receiving antenna ($N = 1$). An interpretation for the UWB MIMO system's superior SEP performance over the narrowband MIMO system is that the UWB channel's inherently large diversity order has the effect of random coding functions in its impulse responses. Thus, the UWB channel's impulse responses in general are linearly independent functions.

Having assumed perfect channel knowledge and a matched filter corresponding to the all-Rake receiver as described in [17], our results should be interpreted as indications of potential performance gains for practical systems.

Acknowledgment

We thank D. Schafhuber and F. Hlawatsch of the Vienna University of Technology, W. Utschick of the TU-Munich, and S. Furrer of the IBM Zurich Research Laboratory, for helpful discussions.

References

[1] Federal Communications Commission (FCC). Revision of Part 15 of the commissions rules regarding ultra-wideband transmission systems. *First Report and Order*, ET Docket 98-153, FCC 02-48, adopted on Febr. 14, 2002, released on April 22, 2002. [Online]. Available: http://www.fcc.gov

[2] *Proc. 2002 IEEE Conf. on Ultra Wideband Systems and Technologies*, Baltimore, May 2002, IEEE Catalog No. 02EX580.

[3] W. Hirt, "Ultra-wideband radio technology: Overview and future research," *Computer Communications*, vol. 26, pp. 46–52, Jan. 2003.

[4] M. Z. Win and R. A. Scholtz, "Impulse radio, how it works," *IEEE Commun. Lett.*, vol. 2, no. 2, pp. 36–38, Feb. 1998.

[5] ——, "On the energy capture of ultra-wide bandwidth signals in dense multipath environments," *IEEE Commun. Lett.*, vol. 2, no. 9, pp. 245–247, Sept. 1998.

[6] F. Ramirez-Mireles, "On the performance of ultra-wide-band signals in Gaussian noise and dense multipath," *IEEE Trans. Veh. Technol.*, vol. 50, no. 1, pp. 244–249, Jan. 2001.

[7] D. Cassioli, M. Z. Win, F. Vatalaro, and A. F. Molisch, "Performance of low-complexity rake reception in a realistic UWB channel," in *Proc. IEEE ICC-02*, May 2002, pp. 763–767.

[8] D. Cassioli, M. Z. Win, and A. F. Molisch, "The ultra-wide bandwidth indoor channel: from statistical model to simulations," *IEEE J. Select. Areas Commun.*, vol. 20, no. 6, pp. 1247–1257, Aug. 2002.

[9] H. Lee, B. Han, Y. Shin, and S. Im, "Multipath characteristics of impulse radio channels," in *IEEE VTC*, vol. 3, Tokyo, Spring 2000, pp. 2487–2491.

[10] L. Yang and G. B. Giannakis, "Space-time coding for impulse radio," in *Proc. 2002 IEEE Conf. on Ultra Wideband Systems and Technologies*, Baltimore, May 2002, pp. 235–239.

[11] M. Z. Win and R. A. Scholtz, "Ultra-wide bandwidth time-hopping spread-spectrum impulse radio for wireless multiple-access comunications," *IEEE Trans. Commun.*, vol. 48, no. 4, pp. 679–691, Apr. 2000.

[12] J. Kunisch and J. Pamp. (2002, June) Radio channel model for indoor UWB WPAN environments. 02281r0P802-15_SG3a-IMST-Response-Call-Contributions-UWB-Channel-Models.pdf. Proposal for IEEE P8002.15.3a channel model. [Online]. Available: http://grouper.ieee.org/groups/802/15/pub/2002/Jul02/

[13] M. Z. Win and R. A. Scholtz, "On the robustness of ultra-wide bandwidth signals in dense multipath environments," *IEEE Commun. Lett.*, vol. 2, no. 2, pp. 51–53, Feb. 1998.

[14] J. G. Proakis, *Digital Communications*, 3rd ed. New York: McGraw-Hill, 1995.

[15] W. van Etten, "Maximum likelihood receiver for multiple channel transmission systems," *IEEE Commun. Mag.*, vol. 24, pp. 276–283, Feb. 1976.

[16] E. A. Lee and D. G. Messerschmitt, *Digital Communication*, 2nd ed. Boston (MA): Kluwer, 1994.

[17] M. Z. Win, G. Chrisikos, and N. Sollenberger, "Performance of Rake reception in dense multipath channels: Implications of spreading bandwidth and selection diversity order," *IEEE J. Select. Areas Commun.*, vol. 18, no. 8, pp. 1516–1525, Aug. 2000.

[18] J. Kunisch and J. Pamp, "Measurement results and modeling aspects for the UWB radio channel," in *Proc. 2002 IEEE Conf. on Ultra Wideband Systems and Technologies*, Baltimore, May 2002, pp. 19–23.

[19] R. J. C. Bultitude, "Measurement, characterization and modeling of indoor 800/900 MHz radio channels for digital communications," *IEEE Commun. Mag.*, vol. 25, no. 6, pp. 5–12, June 1987.

[20] D. Greenwood and L. Hanzo, "Characterization of mobile radio channels," in *Mobile Radio Communications*, R. Steele, Ed. London: Pentech, 1992, pp. 92–185.